Applied Energy 376 (2024) 124305

Contents lists available at ScienceDirect

Applied Energy

journal homepage: www.elsevier.com/locate/apenergy

Evaluation of the ducted fuel injection concept for medium duty engines and multi-hole nozzles: An optical analysis

José V. Pastor, Carlos Micó *, Felipe Lewiski, Usama Bin-Khalid

CMT – Clean Mobility & Thermofluids, Universitat Politècnica de València, Camino de Vera s/n, 46022, Valencia, Spain

HIGHLIGHTS

- DFI concept applied to medium duty optical engine with 8-hole nozzle injector.
- The influence of geometrical characteristics of the duct is analyzed in detail.
- DFI reduces overall soot net formation with all duct geometries tested.
- Soot reduction levels limited by small bore size and number of nozzle orifices.

GRAPHICAL ABSTRACT

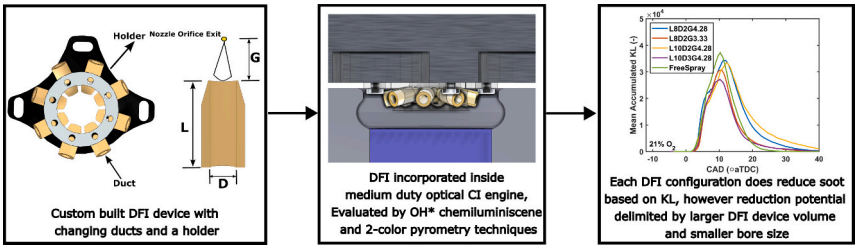

ARTICLE INFO

Keywords:
Ducted fuel injection
Compression ignition
Soot
NO_x
Optical techniques
Combustion

ABSTRACT

Ducted Fuel Injection (DFI) is a strategy still in development, which has proved to be effective in reducing soot emissions in compression ignition engines. It works by driving the spray, formed by a high-pressure fuel injection, through a small duct co-axial to the spray itself, which is expected to affect the mixture formation and combustion process, in turn leading to noticeable reduction in soot formation. This strategy has been mostly deployed in spray vessels or in some cases in heavy duty engines consisting of mostly 2-to-4-hole nozzle injectors. For this reason, the work here is aimed to study the potential of DFI in a medium-duty single-cylinder optical engine fueled with conventional diesel having an 8-hole nozzle injector. Two different optical techniques including OH* chemiluminescence and 2-color pyrometry have been utilized to perform the analysis regarding combustion evolution and soot formation. A parametric analysis regarding different geometrical parameters including stand-off distance, diameter and length of duct has been carried out regarding the DFI performance. Results indicate that DFI does decrease the soot emissions in the context of this study and the duct geometrical parameters influence combustion evolution and soot formation ultimately affecting the device's performance. However, the scale of soot reduction is not as high as reported in previous studies, which is limited by specific boundary conditions including combustion chamber design, piston geometry utilized in this study.

1. Introduction

Pollutant emission mitigation is mandatory to ensure the sustainability of internal combustion engines (ICE) in the short and medium term. Different proposals arise among the research community and the industry, which try to explore the potential of new fuels or advanced hardware designs to minimize the formation of these harmful species during the combustion event. In this context, special attention and

* Corresponding author.
E-mail address: carmirec@mot.upv.es (C. Micó).

https://doi.org/10.1016/j.apenergy.2024.124305
Received 20 October 2023; Received in revised form 15 July 2024; Accepted 19 August 2024
Available online 24 August 2024

efforts are being dedicated to reducing or avoiding the formation of nitrogen oxides (NO_x) as well as soot.

Within this framework, the Ducted Fuel Injection (DFI) concept was first proposed by Mueller et al. [1]. It consists of driving the spray, formed by a high-pressure fuel injection, through a small duct co-axial to the spray itself. They reported the first evidence of the DFI performance in a constant volume combustion vessel (CVCV), with a single-hole nozzle and utilizing natural luminosity (NL) and excited state hydroxyl radical (OH*) chemiluminescence. Their results showed that this new concept was able to enhance air-fuel mixing, resulting in a leaner combustion with much lower soot formation than that observed with a conventional configuration. Gehmlich et al. [2] continued the previous work providing more insight into the effects of this new concept. The authors reported that the DFI caused an increase of the ignition delay (ID) and the lift-off length (LOL), while reaching up to 35–100% of soot reduction over a wide range of operating conditions. Fitzgerald et al. [3] confirmed that the DFI provided longer ID but also faster initial jet penetration. This resulted in a larger LOL, where equivalence ratios were lower than those found at the LOL for a Free spray (FS) configuration. Other authors have also evaluated the impact of DFI on spray development. Liu et al. [4] explored the influence of the device over a wide range of ambient and injection pressures, concluding that an increase of spray penetration was observed specially for high injection pressures. In addition, the authors also reported an increase of the spray cone angle. Fitzgerald et al. [5] performed mixture fraction measurements of diesel sprays with DFI. Authors stated that there was little evidence that mixing is enhanced within the duct. Although the primary effect of the duct was apparently a reduction in the spray cross-sectional area that manifests as higher mean jet velocities and longer lift-off lengths. Their findings were in contrast to the previous claims that DFI improves mixing inside the duct. However, study done by authors in [6] on the fuel spray characteristics and air/fuel mixing of the DFI concept confirmed that mixing is improved further highlighting an intensification of the turbulent mixing when compared to FS. These authors also report a reduction of soot up to 80% when using this new technology. A recent study by Segatori et al. [7] also confirmed that the mixing is indeed improved inside the duct by using DFI. So, all in all, most of the results suggested an improvement of the air-fuel mixing process, as was suggested in most previous works.

One of the main aspects that has been identified as critical for the DFI performance is its geometry. Gehmlich et al. [2] reported that the duct length (L) $>$ 8 mm had minimal effects on DFI performance. However, additional features like a rounded inlet flange provided improvement because it allowed a jet pumping effect that increased the air entrainment driven into the duct. The results by Svensson et al. [8] confirmed the benefits of the DFI concept, however, in contrast, they reported that larger ducts were better at soot reduction as compared to smaller ducts in terms of length. Svensson et al. [8] also reported a decrease of soot luminosity when the axial distance between nozzle orifice exit and duct inlet plane (G, or stand-off distance) was decreased. This was in agreement with the conclusions of Gehmlich et al. [2], who also highlighted that a much smaller axial gap (G $<$ 2 mm) could actually reverse this relation because it will limit the entrainment of the air into the duct, resulting in higher soot formation. In contrast, Li et al. [9] reported that larger G increased the spray velocity which would result in better DFI performance in terms of soot reduction. In the same way, Nilsen et al. [10] while conducting study inside a compression ignition (CI) engine found that larger G duct provided higher soot attenuation. However, they compared 1.6 mm and 3 mm G distance, which is close to the range limits proposed in [2]. Li et al. [9] also explored the impact of duct inner diameter (D). Their findings indicated that a narrower duct exhibits better spray diffusion, longer liquid length and a broader spray cone angle which would result in better DFI performance. Further, in other studies [4,11] they confirmed that a smaller D performs better, provided that spray diameter doesn't exceed that of duct inlet. More recently, Svensson et al. [12] conducted an experimental study in order to find an optimum duct size to be utilized with DFI concept. They also highlighted the importance of ambient temperature, playing a key role in DFI performance. Besides, they confirmed that DFI efficacy in reducing soot formation is decreased when increasing D and ambient temperature.

The first study inside a CI engine related to DFI was performed by Nilsen et al. [10] where authors studied DFI performance inside a 1.7 l single cylinder heavy duty optical CI engine operating under skip fire mode with 2 orifice injector nozzle having rather smaller diameter of 110 μm at injection pressure of 180 MPa utilizing NL imaging technique. DFI was effective in curtailing soot emissions and also in terms of breaking the soot-NO_x trade off. This study proved the efficacy of DFI concept to reduce soot emissions in engine application and matched the previous results of spray vessels. Nilsen et al. [13] presented later, a similar work with 4 orifice fuel injectors. Their study was conducted on a wide range of operating conditions including injection pressure sweep, intake oxygen mole fraction sweep, injection duration sweep, start of combustion timing (SOC) sweep, intake pressure and temperature sweep. They concluded that DFI decreased the soot emissions in all the operating conditions tested. Wilmer et al. [14] performed experiments in the same optical engine as used by authors in [10,13] with a 4 orifice injector nozzle having diameter of 175 μm to measure the particulate matter (PM) and particulate number (PN) for DFI and FS using an engine exhaust particle sizer and a photoacoustic analyzer. Results highlighted that total solid particle concentration and PM were reduced by 59% and 77% respectively, for the case of DFI. Svensson et al. [15] performed experiments with 6-hole nozzle injector having diameter of 205 μm inside a heavy-duty metal engine. As mentioned, this study was performed inside a metal engine in contrast to previous optical engine works and was a step towards right direction in terms of evaluating DFI in real engine conditions. In this case, their results were in contrast with previous literature findings as DFI consistently produced more soot than FS configuration at high loads condition. For this reason, they suggested that a proper design optimization of the combustion system was necessary. The application of DFI was combined with oxygenated fuel blended with diesel by Mueller et al. [16] in the same CI engine as previous work conducted by the same group [10,13]. The authors utilized two blends containing oxygenated fuels alongside conventional diesel fuel at various oxygen concentrations with a two-orifice fuel injector. They were able to achieve a sort of incandescence attenuation of up to around 100 times, indicating DFI combined with oxygenated fuels can curtail soot emissions by a substantial amount. Recently Nyrenstedt et al. [17] studied DFI alongside low net carbon fuels inside a CI engine utilized in [10,13,16] at different oxygen dilution levels and at two different load conditions. Conclusions highlighted that independent of load being used, DFI along with low net carbon fuels can break the soot-NO_x trade off and can be presented as a solution to future stricter emissions regulations.

In parallel to the experimental work done related to DFI, a series of numerical investigations has been also carried out by different authors in order to better understand the DFI concept. A numerical investigation of DFI and FS was carried out by Liu et al. [18] where authors simulated DFI and FS under CI engine conditions using n-dodecane as diesel surrogate. Their conclusions were in line with previous literature, highlighting that DFI strategy reduced the combustion duration and increased the ignition delay. In fact, the use of this new concept increased the low-temperature heat release region and decreased the high-temperature one, leading to soot reduction. Piano et al. [19] investigated the DFI device inside a light duty diesel engine at various engine operating points. Despite observing a reduction of soot formation, they identified certain oxidation problems. For this reason, they highlighted that a proper optimization of combustion system would be necessary before the full advantage of DFI in terms of soot mitigation can be obtained. Recently, another numerical study related to DFI was performed by Sener et al. in [20,21] where authors findings complemented the experimental literature results. DFI was able to achieve up to 66.7% attenuation in soot with respect to FS and it was also effective in decreasing carbon monoxide (CO) and hydrocarbon (HC)

emissions.

Taking into account all the work done on Ducted fuel injection (DFI) concept, it is understood that DFI can attenuate soot emissions and can break the soot-NO_x trade off in most cases. However, the studies conducted so far are limited to spray vessels and heavy-duty engines utilizing 2-to-4-hole nozzle injectors and have shown some limitations when this number has been increased up to 6 holes. In addition, among the different studies there are contradictory conclusions regarding the influence of the main geometrical parameters of DFI. Hence, there is still a need to better understand the way the DFI works inside an engine and how the different geometrical parameters affect the DFI performance. For this reason, the work presented in this study proposes a new scope of application to DFI concept, where a medium duty single cylinder optical engine with 0.8 l capacity is utilized with an injector fueled with conventional diesel and 8-hole nozzle. Hence, the work presented here is unique in its perspective due to the following reasons. Primarily, the use of an 8-hole injector for the first time alongside DFI provides a new scope towards the use of this promising technology, much closer to current commercial applications. Furthermore, due to the smaller design of the combustion system, the distance between the DFI outlet and the bowl wall is reduced, which has consequences on the DFI performance not explored previously. Four duct designs with different geometrical dimensions have been utilized in this study in order to evaluate the influence of DFI geometry in this new scenario. It comprises the change of stand-off distance (G), length (L), and inner diameter (D), allowing to identify an optimum geometry for this application. DFI performance has been analyzed by the use of two different optical techniques including OH* chemiluminescence and 2-color pyrometry at three different oxygen concentrations (21%, 18% and 15% O_2). The results suggest that the performance of DFI depends on these geometrical parameters. A combination of larger stand-off distance with longer length and bigger diameter provides itself an optimum combination to reduce soot during this application. However, in contrast to the results in literature, the high soot reduction levels previously reported have not been observed here. The DFI performance seems to be limited by the specific boundary conditions of the study (including combustion system geometry and dimensions).

2. Experimental setup and methodology

The experimental setup consists of several parts including the ducted fuel injection device, optical engine, relevant operating conditions, optical techniques and the post-processing methodology utilized. These are described in the following subsections.

2.1. Ducted fuel injection (DFI) device

The DFI design developed on purpose for this study consisted of two distinct parts named holder and ducts (Fig. 1). The holder is attached to the cylinder head which ensures the same alignment throughout the experimental campaign, while the different ducts can be removed and replaced. The holder was built of stainless steel while an aluminum alloy was used for the ducts which were black anodized in order to avoid undesired reflections from the soot radiation.

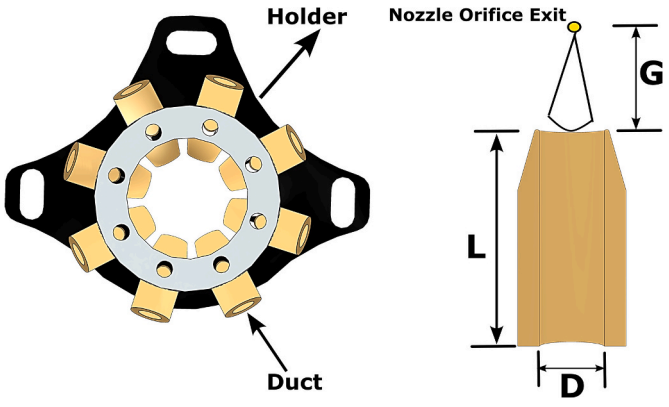

Fig. 1. DFI device along with Duct and Holder.

The flange at the inlet orifice of the duct was rounded in order to gain advantage of pumping effect as suggested by Gehmlich et al. [2]. Ducts with four different combinations of length, diameter and the stand-off distance were tested. These dimensions are indicated in Fig. 1. From here onwards in the manuscript, the four duct designs will be identified by the nomenclature L##D##G##, including the value of each dimension. The proposed designs are presented in Table 1.

The combinations of L, D and G were chosen based on previous literature research where many authors reported different dimensions but falling in a similar range. In addition, the dimensionless parameters named insertion (K_{ins}) and engagement (K_{eng}) co-efficient defined in [1,2] as well as the G/D ratio were used as reference to compare with previous proposals. The first one represents the axial distance from duct inlet to first contact point between spray and duct wall and is non-dimensionalized by dividing it by duct inner diameter. Similarly, the second one is defined as the axial distance over which spray would interact with duct wall and is again non-dimensionalized by dividing it by duct inner diameter. Table 2 shows a summary of the comparison of K_{eng} and K_{ins} between the designs studied in this work and other proposals from literature. Here φ represents the spray cone angle in degrees.

It can be seen that the dimensionless parameters considered as reference are comparable with those of other designs in literature. Only the one identified as L10D3G4.28 has lower K_{eng}value compared to all other designs. In addition, it must be highlighted that a rather larger G was used in this study as compared to literature. The possible collision between ducts at their inlet region due to the large number of nozzle holes limited the use of a smaller G. Similarly, the possible interference with valves limited the maximum length to 10 mm.

2.2. Optical engine

Experiments were carried out in a single cylinder medium duty optical engine with a capacity of 0.8 l (Fig. 2). This engine is an overhead valve (OHV) type and has 2 intake and 2 exhaust valves per cylinder inside the cylinder head. It has been extensively described in previous works [22–25]. However, a few important details are included here for readers convenience. An electric dynamometer was used to motor the engine. To achieve the required intake air pressure, a screw compressor was employed, and a valve located in the exhaust pipe was used to simulate a backpressure of 0.2 bar compared to the intake. Moreover, an air heater, positioned just before the intake port, ensured the intake air reached the desired temperature. A piezoelectric transducer (Kistler-6124 A) was utilized to obtain the in-cylinder pressure. Similarly, piezoresistive transducers (Kistler-4049A5) were used to measure the instantaneous intake and exhaust pressures. An oscilloscope (Yokogawa DL708E) which was synchronized with a crankshaft encoder, recorded the pressure signal, providing a 0.5 crank angle degree (CAD) resolution. The measured in-cylinder pressure was used to calculate the apparent heat release rate (aHRR) by applying the standard first-law thermodynamic analysis [26].

Table 1
Description of different duct designs utilized.

Duct Design	Length (L) [mm]	Diameter (D) [mm]	Stand-off distance (G) [mm]
L8D2G4.28	8	2	4.28
L8D2G3.33	8	2	3.33
L10D2G4.28	10	2	4.28
L10D3G4.28	10	3	4.28

Table 2
Comparison of dimensionless parameters between duct designs found in literature and utilized in this work.

Duct Design	L [mm]	D [mm]	G [mm]	φ [°]	G/D [−]	K_{ins} [−]	K_{eng} [−]
Gehmlich et al. [2]	6	1.5	3.25	15	2.17	1.631	2.369
Gehmlich et al. [2]	14	3	4	21	1.33	1.364	3.302
Millo et al. [6]	14	2	1	13	0.50	3.888	3.112
Svensson et al. [8]	14	2	2.2	15	1.1	2.697	4.302
L8D2G4.28	8	2	4.28	15	2.14	1.658	2.342
L8D2G3.33	8	2	3.33	15	1.67	2.133	1.867
L10D2G4.28	10	2	4.28	15	2.14	1.658	3.342
L10D3G4.28	10	3	4.28	15	1.43	2.371	0.962

For the purpose of this study, a few modifications were made on the cylinder head. Holes were drilled on the head to attach the DFI. In terms of optical access, it was achieved through a piston extensor, which was used to hold the quartz piston on top of it. A standard 8-hole conical nozzle was used with orifice diameter of approximately 138 μm, with a common rail delivering the fuel to injector. Furthermore, a re-entrant piston with flat bowl was used in this work, in order to minimize optical distortion. Fig. 2 also shows the sketch of the facility along with a cut section view of the utilized piston with DFI installed. The main parameters of the engine are listed in Table 3.

2.3. Operating conditions

A skip fire mode was chosen to operate the engine which means only 1 out of 20 cycles was a firing cycle. This ensured a proper renovation of in-cylinder air during each cycle before start of combustion (SOC), while limiting the thermal stress applied upon the engine and the different parts. Furthermore, to cancel out the effect of cycle-to-cycle variability on the analysis, ten successive combustion cycles were recorded. In terms of fuel, standard diesel was used, which properties are enlisted in Table 4.

The purpose of this study was to evaluate the effect of different DFI parameters on its performance and compare it with Free Spray (FS), so a rather simpler injection strategy consisting of one main and one pilot injection was utilized. The energizing signal is represented in Fig. 3.

Table 5 summarizes the main operating conditions utilized in this work. It should be noted that the same three tests were performed for four DFI configurations as well as FS. It corresponded to 7.6 bar indicated mean effective pressure (IMEP), which can be considered medium load conditions. In addition, three different oxygen concentrations i.e., 21%, 18% and 15% O_2 were used in order to simulate the effect of exhaust gas recirculation (EGR). This reduction in O_2 concentration was accomplished by the dilution of airflow with nitrogen at the intake port.

It is worth mentioning that the presence of DFI modifies the compression ratio. Thus, the intake pressure was increased to 1.37 bar for the FS cases to reach the same in-cylinder pressure at the moment of the fuel

Table 3
Optical engine parameters without DFI.

SCE Technical Data	
Operational mode	Compression ignition engine
Number of cylinders	1
Number of valves [−]	4
Bore [mm]	103
Stroke [mm]	99
Displacement [l]	0.8
Effective compression ratio [−]	13.3
Connecting rod length [mm]	163.63

Table 4
Properties of utilized fuel.

Parameter	Value
Fuel [−]	Diesel
Viscosity @ 40 °C [mm^2/s]	2.59
Density [kg/m^3]	829.2
Cetane number [−]	52
Lower heating value [MJ/kg]	41.92

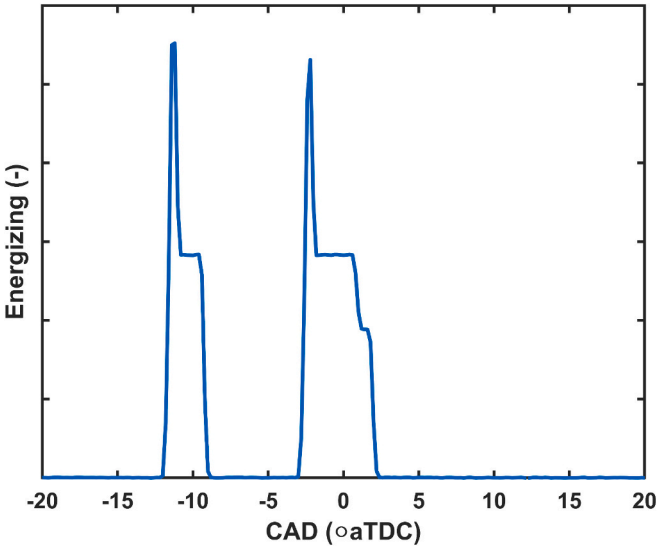

Fig. 3. Energizing signal utilized for injection.

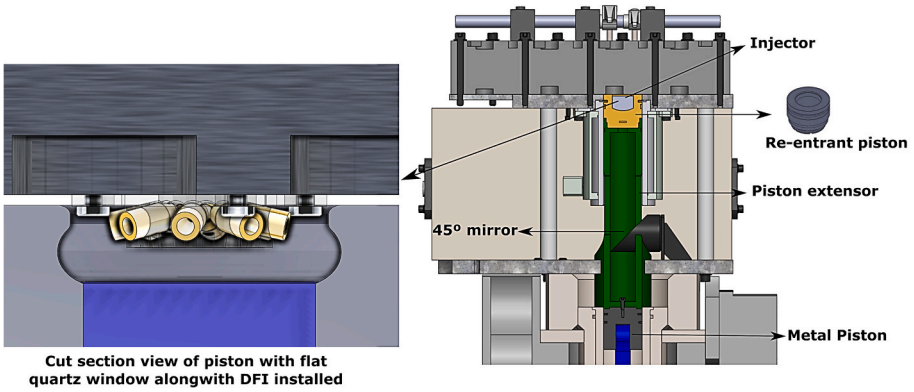

Fig. 2. Different components of optical engine utilized.

Table 5
Summary of operating conditions utilized.

Parameter	All DFI Configurations			Free Spray Configuration		
Oxygen concentration [% O2]	21	18	15	21	18	15
Indicated Mean Effective Pressure (IMEP) [bar]	7.6	7.6	7.6	7.6	7.6	7.6
Engine speed [rpm]	1200	1200	1200	1200	1200	1200
Intake temperature [°C]	55.4	55.4	55.4	55.4	55.4	55.4
Intake pressure [bar]	1.34	1.34	1.34	1.37	1.37	1.37
Exhaust pressure [bar]	1.54	1.54	1.54	1.54	1.54	1.54
Injection pressure [bar]	1200	1200	1200	1200	1200	1200
Start of energizing (SOE) [CAD after top dead center] [°aTDC]	−12	−12	−12	−12	−12	−12

injection.

2.4. Optical techniques

Two different optical techniques including OH* chemiluminescence high speed imaging and 2-color pyrometry were utilized in order to analyze the combustion development inside the engine. Fig. 4 shows the setup used in this work.

Flame radiation coming from the quartz piston bottom gets reflected by the 45-degree elliptical mirror and then reaches this optical setup. The very first element in the optical setup is a dichroic mirror which transmits the visible radiation and reflects the ultraviolet (UV) radiation. The range of the UV radiation reflected by dichroic mirror falls in line with the most intense excited state hydroxyl (OH*) radical emission band which is 310 nm. This reflected UV radiation is then registered by an intensified high-speed camera equipped with a narrow band interference filter. The visible light that goes through the dichroic mirror then reaches beam splitter which reflects half of the light and transmits the other half. These two halves of the visible light are then registered by two high speed cameras as shown in the Fig. 4 i.e., 550 nm and 660 nm camera. Both of these high-speed cameras are equipped with a specific narrowband interference filter which registers only specific wavelength i.e., 550 nm and 660 nm having a full width at half maximum (FWHM) of 10 nm, necessary for 2-color pyrometry algorithm. In order to ensure the image-by-image correlation among the three different images registered, the three cameras were simultaneously triggered with the start of energizing (SOE) and were synchronized on the basis of frame.

- **OH* Chemiluminescence**

The OH* radical is termed as a good tracer for the high temperature reactions in a diffusion combustion [27]. Therefore, in order to trace the near stoichiometric high temperature zones inside the piston, OH* chemiluminescence high speed imaging was utilized. For the purpose of this technique, a Photron Fastcam SA-5 high speed camera equipped with Hamamatsu C10880—03F high-speed intensifier was utilized. This high-speed camera as mentioned earlier was equipped with a narrow-band interference filter having a central wavelength of 310 nm and a 10 nm full width half maximum (FWHM). The purpose of this filter was to selectively capture only the radiation corresponding to the OH* emission peak while rejecting others. The camera's gating was synchronized with an exposure time of 39.75 μs, and the intensifier gain remained at 62.5% of maximum value for the tests with 21% and 18% O_2, while for the case of 15% O_2 the gain was increased to 87.5% of the maximum value in order to ensure proper visualization which was jeopardized by less oxygen present inside the cylinder. The camera's acquisition speed was set at 25,000 frames per second (fps), ensuring high temporal resolution. Additionally, this camera had a resolution of 4.15 pixels per millimeter.

- **2-Color Pyrometry**

In this study, 2-color pyrometry is employed to measure the amount of soot present within the combustion chamber. This technique involves detecting the thermal radiation emitted by the soot at two distinct wavelengths. The soot surface temperature and its optical density are determined by the application of Plank's law [28] and the combination of these two distinct wavelengths. This working principle of this technique has been extensively explained in previous works [22,29–31]. The principal results in determination of a dimensionless parameter named as KL, which in fact represents the optical soot density and gives information about the total soot present along the optical path of the flame [32].

For the purpose of this technique two Photron NOVA-S9 high speed cameras were utilized. As shown in Fig. 4, after passing through dichroic mirror, the flame radiation was split into 2 halves by means of a beam splitter. These two halves were registered by the above-mentioned two high-speed cameras. Both cameras were configured with a frame rate of 25,000 fps and were equipped with a 100 mm f/2 Karl-Zeiss Makro-planar camera lens. One of the cameras incorporated a narrowband interference filter, which had its transmission peak focused at 660 nm with FWHM of 10 nm. In contrast, the other camera utilized a filter

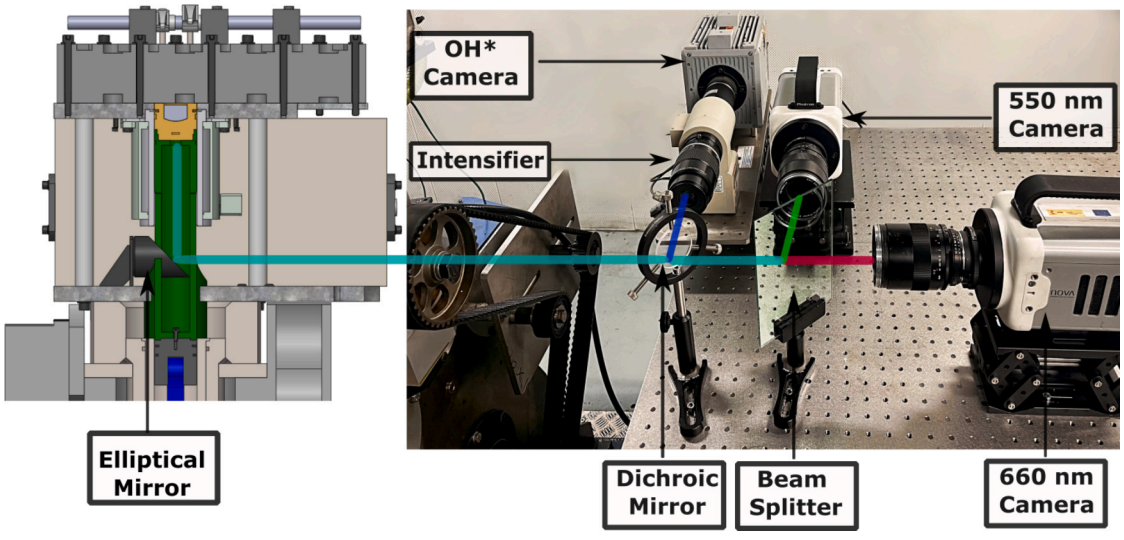

Fig. 4. Optical setup utilized.

centered at 550 nm with a 10 nm FWHM. These two cameras are labeled as 660 nm camera and 550 nm camera in the Fig. 4. Each camera was synchronized with a specific exposure time in order to get the most out of the dynamic range of cameras.

Both images are combined pixel by pixel in order to apply the plank's law of black body radiation as discussed above, to obtain the KL spatial evolution. An in-house MATLAB developed code is utilized for this purpose. Further details can be found at [22,29–31]. Fig. 5 shows the steps involved in the methodology to obtain the Accumulated KL evolution, where 2 raw images from both cameras are combined pixel by pixel applying plank's law to obtain the spatial KL image. Eq. 1 is further used to determine the Mean accumulated KL ($\overline{KL}_{acc}$) evolution, which in in fact the mean of the Accumulated KL ($\sum KL$: sum of all soot pixels) for 10 combustion cycles (here represented by repetitions).

$$Mean\ Accumulated\ KL\ (\overline{KL}_{acc}) = \frac{(\sum KL)_{repititions}}{no.of\ repititions} \tag{1}$$

Furthermore, the temporal and spatial analysis of soot formation and oxidation is carried out by creating the radial maps as shown in Fig. 5. The details of the procedure followed to create the radial maps can be found in previous published work at [22,29,31]. A brief description, however, can be added here for readers convenience. The KL registered images, which are in fact an average of ten combustion cycles, are divided into rings of 0.5 mm radius. Mean of KL for each ring ($KL_{mean\ r}$) is obtained using the Eq. 2, where $KL_{Accumulated\ r}$ is sum of all soot pixels in the specific ring and A_r represents the total amount of pixels present in that certain ring.

$$KL_{mean\ r} = \frac{KL_{Accumulated\ r}}{A_r} \tag{2}$$

Finally, this information regarding mean KL of each ring is summarized into spatial and temporal maps, where the column corresponds to all the ring regions into which the images were divided, which are in fact the respective of distance from the nozzle and the row depicts the registered instants i.e., CAD. The same procedure is followed for building OH* radial maps.

3. Results and discussion

3.1. DFI vs free spray

Discussion can be started by looking at the effect of the DFI device when compared to a FS configuration. For this purpose, duct L8D2G4.28 is chosen as baseline design. Fig. 6 shows the in-cylinder pressure and rate of heat release (RoHR) signal for the case of 21% O_2 concentration along with standard deviation of respective signal highlighted by shaded region which highlights the cycle to cycle variability of measurements.

It can be observed that there are not so many differences between DFI and FS in terms of global combustion behavior. Further, the differences observed are in similar order of magnitude as the variability in measurements highlighted in shaded regions. The ignition delay and combustion duration seem to be quite similar in both cases. However,

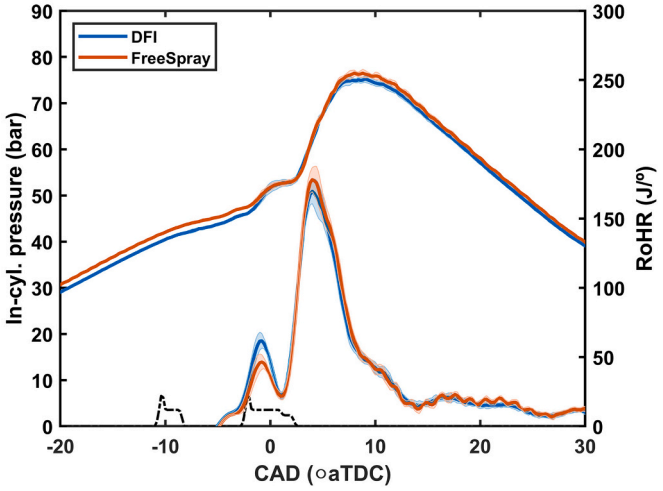

Fig. 6. Comparison of In-cylinder pressure and Rate of heat release signal between base DFI (L8D2G4.28) and Free Spray for 21% oxygen concentration case. Shaded areas around the curves show the standard deviation w.r.t In-cylinder pressure and Rate of heat release.

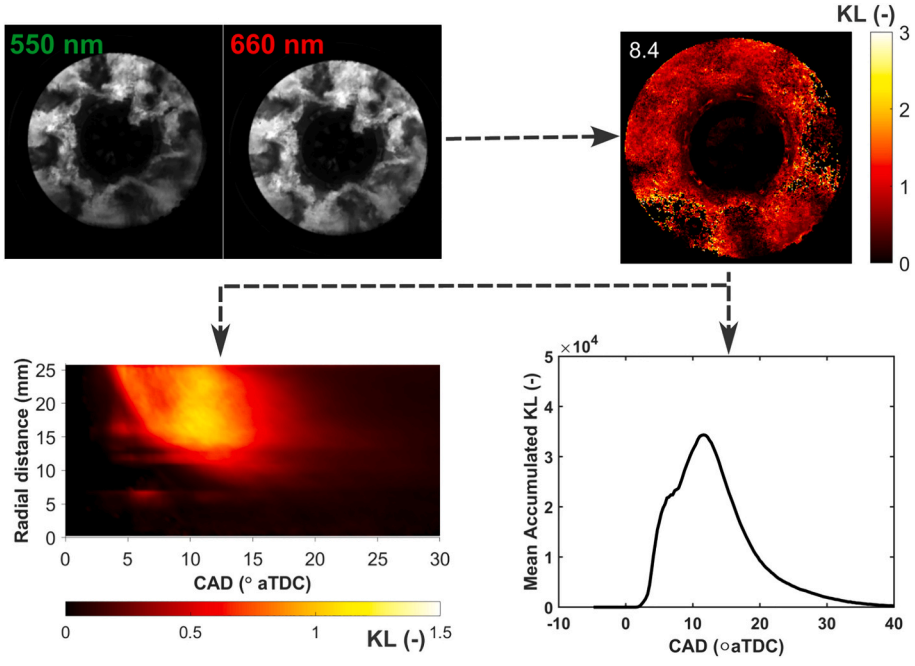

Fig. 5. Description of various steps involved in obtaining KL evolution.

literature have reported that the DFI increases the ignition delay [1,3,8], while combustion duration is decreased. A possible reason after not observing a similar effect in this work is the frequency of the data acquisition. In this work, a measuring resolution of 0.5 CAD was used which was in the order of magnitude of the differences observed thanks to the OH* chemiluminescence signal in this regard. Another reason could be the injection strategy used. On one hand, the pilot injection is burning under premixed regime, in which the DFI effect could be not so noticeable. On the other hand, the first combustion increases temperature and pressure inside the combustion chamber which increases reactivity of the air-fuel mixture and reduces differences between DFI and FS in this regard.

Moving further, by looking at the radiation from combustion, significant differences arise. Fig. 7 shows the OH* and KL images obtained at 4.3 CAD, both for DFI and FS. Focusing on the OH* signal, a clear difference in terms of flame structure and lift-off length is visible between both configurations. DFI increases the LOL and moves the OH* signal towards the bowl wall when compared to FS. This coincides with the literature findings. Another phenomenon which is visible when using DFI is the appearance of weak OH* areas near some duct inlets. This indicates that a small amount of fuel could not be entering into the ducts and is being oxidized there. However, it is a small percentage that is not affecting combustion performance and achieved IMEP.

Fig. 8 shows the $\overline{KL}_{acc}$ for the same DFI design (L8D2G4.28) and FS along with the KL standard deviation highlighted in shaded region. The standard deviation represents cycle-to-cycle variability. It is possible to see that on average for both DFI and FS, the variability around the peak is 3–4% while during the oxidation phase it reaches up to 20–25%. However, it is still lower than the differences observed between DFI and FS. Therefore, it was decided not to include this in further analysis of KL. Moving towards analysis, the first thing that can be observed is that a lower $\overline{KL}_{acc}$ peak is reached with the DFI. At this stage of combustion, when soot levels increase, the formation of this pollutant dominates over its oxidation although both processes are taking place simultaneously. Thus, the lower peak observed indicates a lower net soot formation within the combustion which is in agreement with the soot reductions reported in literature. However, the reduction observed here (in terms of in-cylinder KL) seems to not be as important as the one reported in previous works. A more detailed quantification has been included in further sections.

After the KL peak is reached, the decrease of the KL curve, corresponding to the soot oxidation phase, seems to be delayed for the DFI case as compared to FS. This behavior could be caused by several factors. Primarily the DFI device utilized in this study was relatively larger in volume as compared to the whole combustion chamber. This larger volume could hinder the oxidation of the soot that is re-directed from the re-entrant bowl walls towards the center of the piston, because of less fresh air presence near the DFI device. Contrary to DFI, in the case of FS this reflected soot cloud could be oxidized by fresh air still present at the center of bowl. Piano et al. [19] observed the late oxidation problem of DFI, where they performed a detailed computational fluid dynamics (CFD) analysis under similar operating conditions as those of the present work, including bore/stroke ratio of the considered engine. They stated that the relatively small size of the combustion chamber could hinder the potential of DFI due to earlier interaction of the flame with the bowl wall and later with the device. These findings, which have not been observed previously in bigger engines, are corroborated by the results reported in the current work.

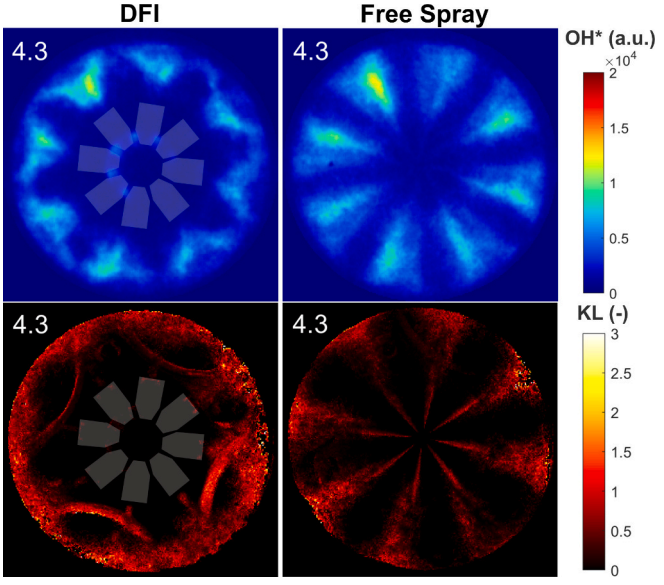

Fig. 7. Comparison of OH* and KL images at 4.3 CAD between base DFI (L8D2G4.28) and Free Spray for 21% oxygen concentration case.

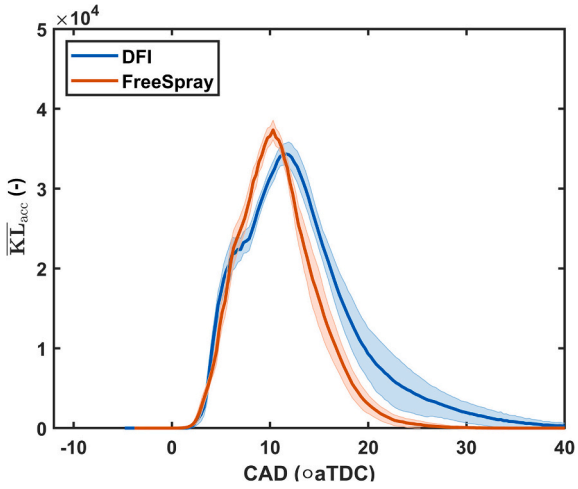

Fig. 8. Comparison of Mean Accumulated KL ($\overline{KL}_{acc}$) signal between base DFI (L8D2G4.28) and Free Spray for 21% oxygen concentration case. Shaded areas around the curves show the standard deviation w.r.t $\overline{KL}_{acc}$.

To get a deeper insight into the OH* and KL spatial evolution, Fig. 9 shows the radial maps for both the cases of DFI and FS, built following the methodology described in the previous section.

The OH* maps highlight the high temperature oxidation activity happening inside the combustion chamber while the evolution of soot is represented by the KL maps. The OH* cloud for the case of DFI, when compared to the FS case, shows intense oxidation activity during the angle span where KL peak is reached (Fig. 8). This leads to a lower $\overline{KL}_{acc}$ (lower soot) in the combustion chamber as reported previously, which suggests that the DFI decreases net soot formation when compared to FS. Moving to later stages of combustion, more differences between both configurations arise. The flame front for FS, as observed in KL maps, seems to be moving closer towards bowl center as compared to DFI. In fact, in the DFI case the soot cloud seems to drastically stop progression between 10 and 5 mm, due to the presence of the device. It is worth mentioning that the outer radius of the holder is close to 12 mm. It can also be observed that, for the FS the higher OH* radiation starts after 10° aTDC in contrast with DFI, where at the same angle the signal starts to decrease. In addition, the region of intense OH* radiation with the FS extends from the periphery of the bowl to almost 10 mm from the nozzle, while with DFI seems to concentrate between 10 and 15 mm. In terms of KL, it is also possible to see that specially in the region between 15 and 25 mm KL seems to disappear faster for the FS case when compared to DFI, with which it is possible to see that KL remains visible during more time. All of this indicates that with FS a higher oxidation activity is achieved during later stages of combustion which leads to a faster soot

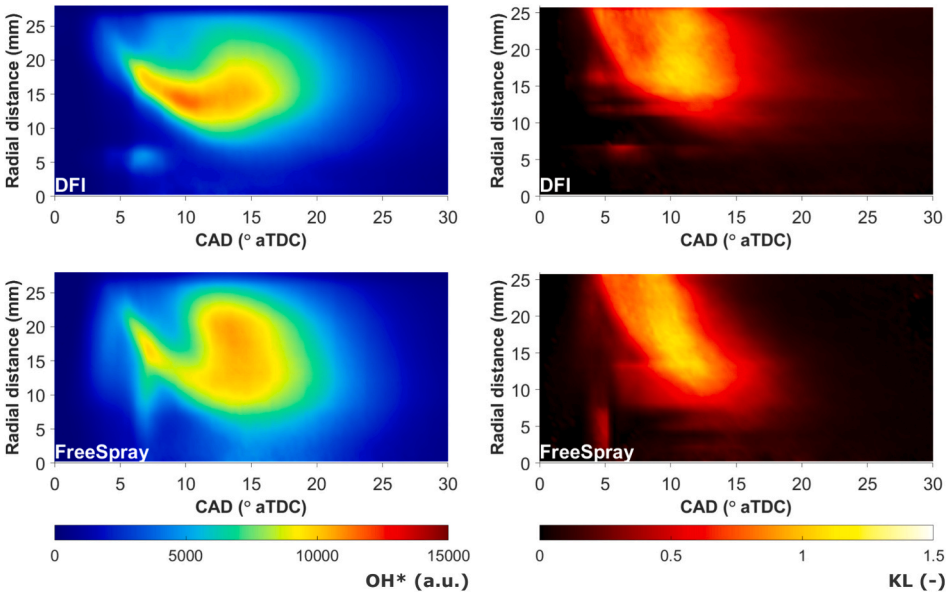

Fig. 9. OH* and KL radial maps obtained for base DFI (L8D2G4.28) and Free Spray at 21% oxygen concentration case.

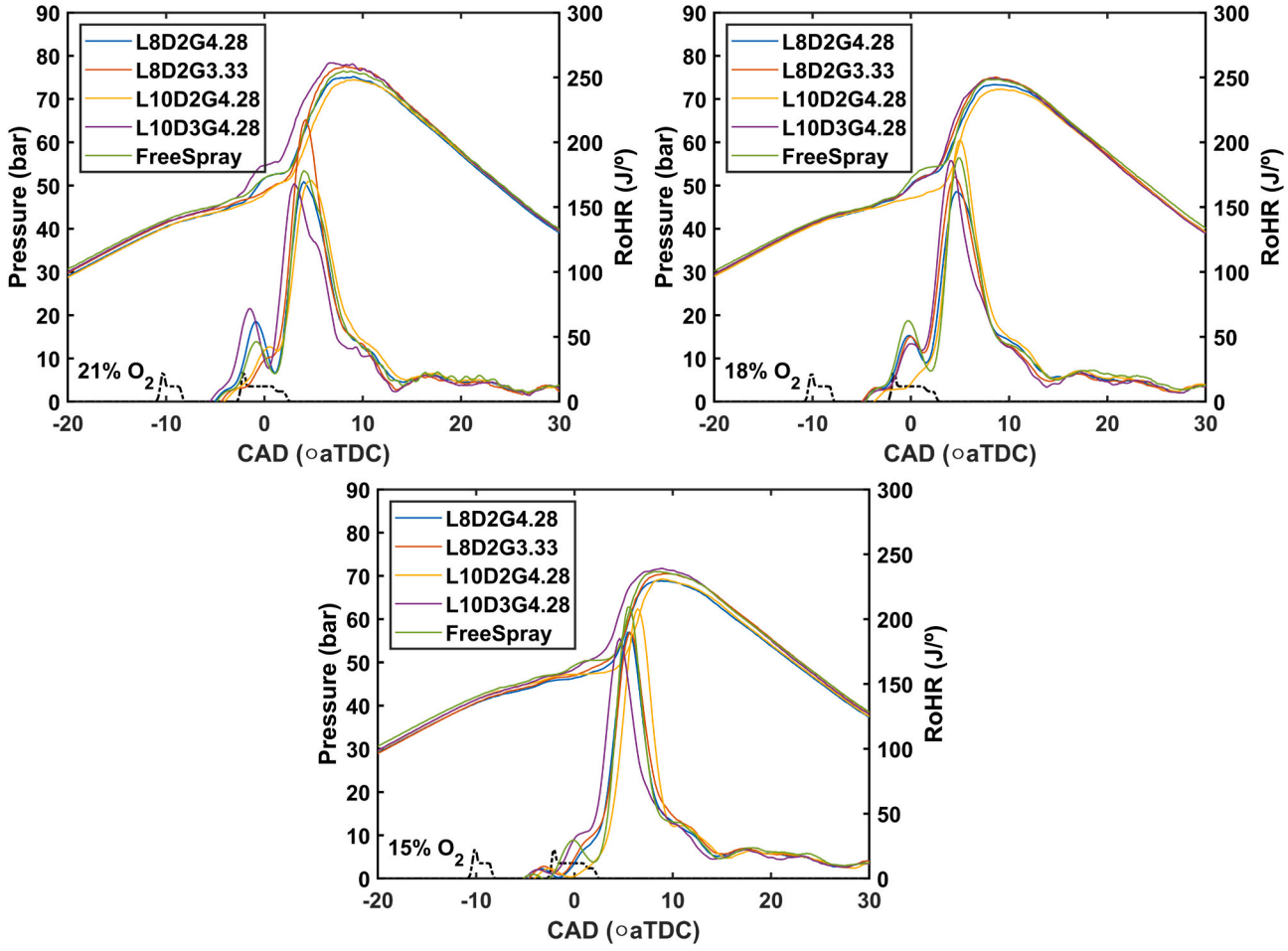

Fig. 10. In-cylinder pressure and Rate of heat release signals for all the ducts utilized and Free Spray configuration including all three oxygen concentrations (21, 18 and 15%).

oxidation in a wider region of the combustion chamber, as it was observed in Fig. 8.

3.2. Parametric evaluation of DFI geometry

As it has been discussed in previous sections, the geometry of the ducts has been identified in literature as a key parameter to optimize the performance of DFI in terms of soot reduction. For this reason, an evaluation of the main geometrical parameters including L, D and G is presented here to better understand their effect on the overall performance of the device in the context of the current work (relatively small bowl diameter and more nozzle holes). Discussion is started by presenting a global overview of geometrical parameters on combustion development and performance. Then, it will be followed by an analysis of soot (KL) and OH* chemiluminescence in the combustion chamber.

- **Thermodynamic analysis**

Fig. 10 shows the in-cylinder pressure and RoHR signals for all the ducts and FS for three different oxygen concentration cases.

Primarily, a clear effect of decreasing the oxygen concentration can be seen with both DFI and FS. The ignition delay is increased as the O_2 concentration is decreased. The energy released by the pilot injection tends to weaken and even disappear in some cases. However, as stated previously, no clear and consistent differences between DFI and FS can be observed in this regard. Only the L10D2G4.28 configurations seem to cause a longer ignition delay for all conditions. With the rest, it can be concluded that combustion evolution is similar to FS.

- **In-cylinder evolution analysis**

In this section, the effect of the duct geometrical parameters on the DFI performance in terms of soot reduction will be analyzed. Fig. 11 shows the $\overline{KL}_{acc}$ obtained for all four different duct configurations and FS in all three O_2 concentration conditions.

In general, all the geometries tested provide a reduction of the KL maximum peak and hence a reduction of soot formation as discussed previously. However, it can be seen that the duct L10D3G4.28 is consistent in reducing maximum KL more than the other designs when compared to FS in all 3 oxygen concentrations cases. The other visible difference among all ducts is the limitations with late oxidation of soot. However, some duct designs seem to improve it when compared to the others. In this regard, the L10D3G4.28 and the L8D2G3.33 provide the best performance as a larger reduction of KL during the oxidation stage is reported.

To look at the spatial evolution of the combustion process, the analysis is complemented with the corresponding OH* and KL radial maps for 21% O_2 (Fig. 12). Thanks to these maps, it is possible to see

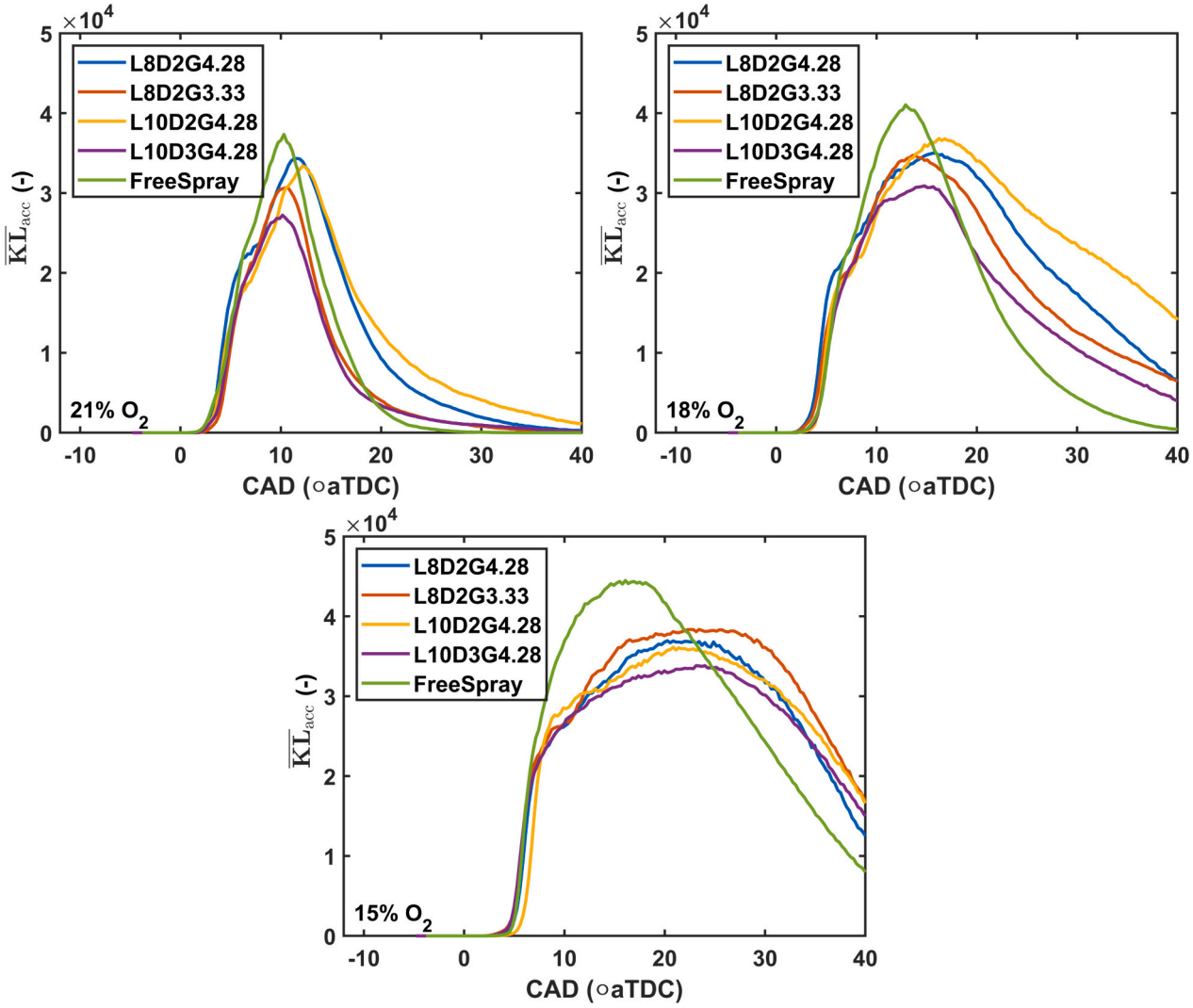

Fig. 11. Mean Accumulated KL ($\overline{KL}_{acc}$) signal for all the ducts utilized and Free Spray configuration including all three oxygen concentrations (21, 18 and 15%).

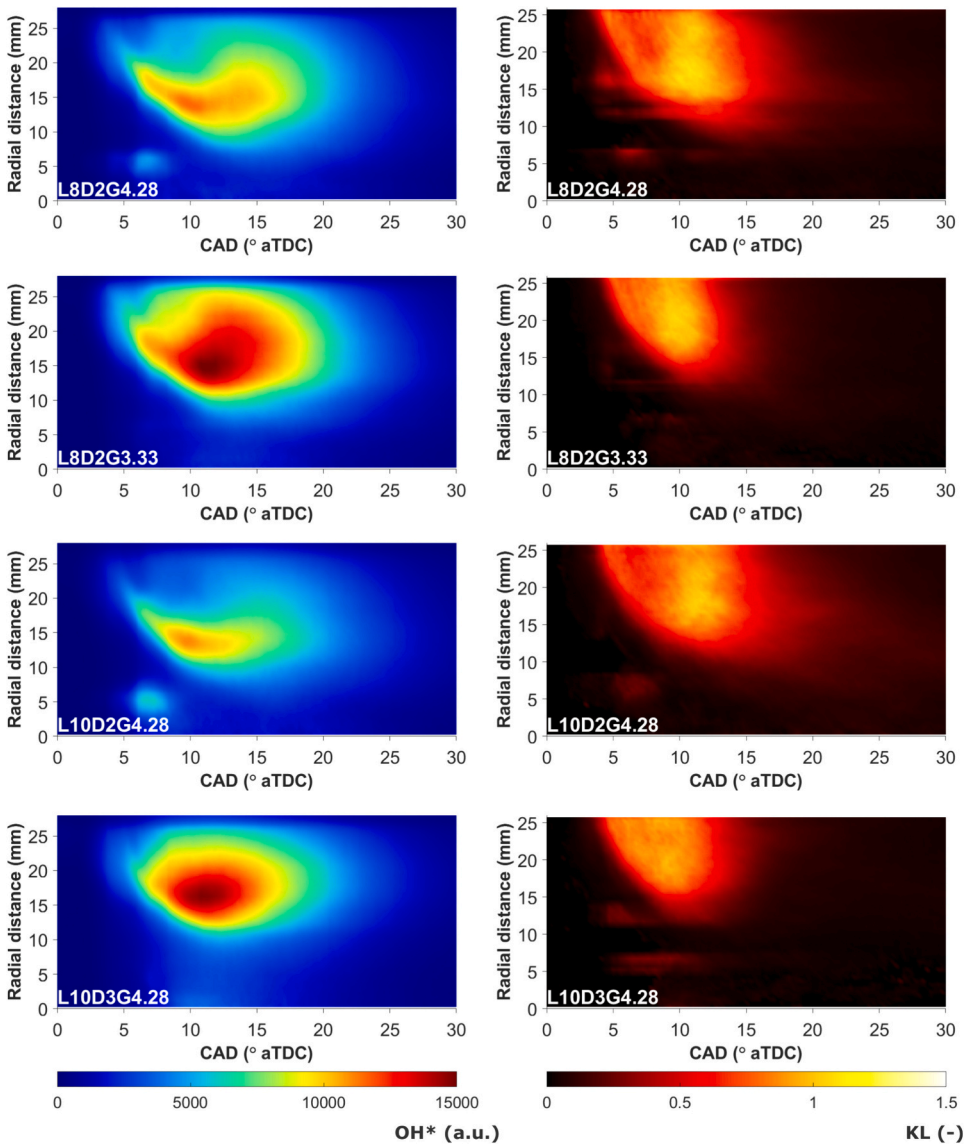

Fig. 12. OH* and KL radial maps obtained for all the ducts utilized at 21% oxygen concentration.

large differences in terms of OH* chemiluminescence among ducts. With L10D3G4.28 and L8D2G3.33, a much more intense activity is observed between 10 and 15° aTDC, extending among a wider region of the piston bowl between 15 and 25 mm radius from nozzle. This is accompanied by a faster reduction of KL when compared to the other two cases, with which KL remains longer in the cycle at positions above 15 mm. The effect of each dimensional parameter has been discussed in more detail in the following paragraphs.

o **Influence of Stand-off Distance (G)**

Looking at the Fig. 11 and focusing on 21% O_2, by only decreasing the stand-off distance (G) from 4.28 mm (blue curve) to 3.33 mm (orange curve), the overall peak of the KL is decreased indicating lower net soot formation inside the cylinder. Improvement is also seen in terms of late oxidation. Therefore, it can be stated that reducing G helps both to reduce the overall KL and the speeding up the late oxidation of soot.

This can be explained by the fact that, as the duct inlet gets closer to the nozzle, the cross section of the spray is smaller at the duct inlet leaving more space and improving air entrainment towards the duct, resulting in better air-fuel mixing and hence a leaner combustion and lower soot formation. These results coincide with the literature, where it has been reported that lower G decreases soot formation while larger G has the opposite effect [2]. However, these authors also highlighted that a much smaller axial gap (G < 2 mm) could actually reverse this relation because it will limit the entrainment of the air into the duct, resulting in higher soot formation. In this sense, Svensson et al. [8] evaluated G in a range from 0.1 to 6 mm in a high temperature pressure vessel reporting similar conclusions despite not observing this change of trend. However, the authors when comparing a short duct with a long stand-off distance (L8D2G4.5) to a longer duct that has a similar duct exit location (L14D2G0.1) concluded that both yield a similar soot reduction result. This implies that the mixing state at the duct exit is comparable, indicating that it makes no difference whether the air was entrained into the jet before the shorter duct entrance or within the longer duct. However, it must be noted that the study was conducted in a vessel with no wall interactions in contrast to the current engine study. Further, it is not possible to draw such conclusions regarding duct exit location as the current study is limited in terms of changing the length and the stand-off distance to that large extent. In applications like the one presented in this work, it is not possible to assemble the ducts so close, especially with multiple nozzle holes. Considering this limitation, it can be concluded that duct should be mounted as close as possible to nozzle exit which, in practice is limited to 3–4 mm for an 8-hole nozzle. Looking at the radial

maps in Fig. 12, it is quite clear when comparing OH* chemiluminescence that decreasing G increases the oxidation activity. This contributes towards the lower KL and faster decrease as discussed previously.

Moving towards lower oxygen concentrations, the trends observed for the case of 21% O_2 seems to hold only for 18% O_2. When reaching 15% O_2, the smaller G seems to become ineffective both in terms of decreasing maximum KL and improving the later oxidation. The current authors consider that the combination of a smaller G and lower oxygen concentration would make it difficult to entrain enough O_2 before duct inlet which would potentially lead to richer mixtures downstream the duct and hence more soot formation than the other duct configuration. The effect would be like the one described in [2] when decreasing G. Therefore, in general it can be stated that the decrement of G, with constant L and D, improves the oxidation activity and results in lower KL peak when compared with longer G as long as oxygen concentration is above 15%.

o **Influence of Duct Length (L)**

In this study, two different duct lengths have been tested: 8 mm and 10 mm. As mentioned in the device description, 10 mm was the maximum possible length to avoid interference with the valves. By looking at the Fig. 11 and focusing first on 21% O_2, small differences can be seen when comparing L8D2G4.28 (blue curve) and L10D2G4.28 (yellow curve). Primarily, when increasing L, the KL maximum peak is delayed and slightly decreased. Regarding late oxidation, the same behavior is observed or even slightly worsened. The OH* chemiluminescence (Fig. 12) shows a slightly less intense region for the longer duct suggesting lower oxidation activity. In addition, KL maps show a wider cloud for longer time indicating slower oxidation of soot. When comparing with literature, authors in [2] reported that no significant differences were observed in terms of soot reduction when duct length was changed from 8 to 16 mm keeping the G and D same. Similar results were observed by Nilsen et al. [33] where the difference in terms of soot attenuation was not significant when comparing larger and shorter ducts. Henceforth, the findings in the current work in terms of net soot formation are consistent with the literature. However, some problems arise for L = 10 mm which have not been observed in other applications.

The trends observed for the case of 21% O_2 are held for 18% and 15% O_2 cases. A longer L provides a slightly lower maximum KL peak but slows down the oxidation process as compared to shorter L. However, the differences reported are subtle.

o **Influence of Duct Diameter (D)**

As it was highlighted previously, the duct L10D3G4.28 provided the best improvement in terms of KL among all the designs tested when compared to FS. Keeping the L and G constant, the $\overline{KL}_{acc}$ evolution curves for L10D2G4.28 (yellow) and L10D3G4.28 (purple) for 21% O_2 can be compared in Fig. 11. A significant reduction is achieved when duct diameter is increased by 1 mm, keeping the other parameters constant. This could be related to the fact that as the nozzle orifice diameter is larger in this work (138 μm), more fuel is injected, and hence more air is required to be entertained at the duct inlet to achieve better mixing. In this regard, a larger diameter of the duct is beneficial. In addition, an improvement in oxidation is also observed. These findings are consistent with literature as reported in [33]. Their results indicated that larger diameter with larger nozzle orifice diameter worked better in terms of soot attenuation as compared to smaller diameter when keeping L and G same. The OH* chemiluminescence maps in Fig. 12 also highlight significant differences in terms of signal intensity. For the case of D = 3 mm, OH* signal is much more intense, highlighting a stronger oxidation activity. This is also reflected in KL evolution maps in Fig. 12, where KL cloud is much smaller and extinguishes faster compared to D = 2 mm, indicating faster oxidation.

The same trend is also observed for 18% and 15% O_2 cases. Hence, in general it can be stated that the increment of D, with constant G and L, results in a lower KL peak and higher oxidation activity when compared with smaller D.

- **Quantification of the reduction of in-cylinder KL achieved with DFI**

In order to get a better understanding of global behavior in terms of reduction in KL by utilizing different ducts, the Mean Accumulated KL ($\overline{KL}_{acc}$) reduction is plotted for all ducts calculated with respect to FS and for three different O_2 concentrations. This reduction has been calculated according to Eq. 3 by subtracting the $\overline{KL}_{acc}$ obtained by each DFI from the FS values and then normalized by the $\overline{KL}_{acc}$ achieved with FS. It must be noted that the calculation is performed per each crank angle degree (CAD).

$$\overline{KL}_{acc}\ Reduction = \frac{\overline{KL}_{acc\,FS} - \overline{KL}_{acc\,DFI}}{\overline{KL}_{acc\,FS}} \tag{3}$$

Fig. 13 shows the $\overline{KL}_{acc}$ reduction evolution obtained for each of the four duct designs utilized in this work and for three different oxygen concentrations discussed previously. In all three cases, it can be seen that the maximum KL reduction is achieved by L10D3G4.28 where it varies from 30 to 35% with respect to FS. In contrast, the worst performance is obtained with the L8D2G4.28 for which the maximum values vary between 15 and 20% and are visible for a shorter range of CAD. The advantages reported for L8D2G3.33 and L10D3G4.28 are related with lower maximum KL achieved but is also observable for a longer part of the combustion cycle (up to 20° aTDC) thanks to the less oxidation difficulties reported. Nevertheless, for all the geometries the KL decreases slower than with FS and, at certain point, measured KL levels become higher, as it can be observed in Fig. 13 when the reduction values become negative. This effect was also reported by Piano et al. [19] under similar geometrical and operating conditions.

4. Conclusions

The DFI concept has been evaluated in a medium duty optical engine with a nozzle having 8 holes. It represents a particular application different from those reported previously in literature. Four different duct designs were utilized in this study among which the most relevant geometrical parameters (G, D and L) were modified to evaluate its influence on DFI performance. The first analysis comparing one of the duct designs (L8D2G4.28) with the FS configuration confirmed the influence of DFI on combustion evolution, especially in terms of spatial development. The results confirmed also that net soot formation was attenuated to around 15–20% but some problems were observed during the late oxidation stage.

When analyzing the influence of G, L and D on DFI performance, the following conclusions can be established:

- Reduction of stand-off distance (G), improves the late oxidation and also decreases the maximum KL peak. This agrees with the results observed in literature in larger engines and combustion vessels. However, some limitations have been observed when O_2 concentration is reduced below 18%.
- Increment in duct length (L), has almost no effect on reducing net soot formation (KL peak) and worsens the oxidation.
- Increasing the duct diameter (D), improves the late oxidation to quite extent and decreases the maximum KL peak. This behavior is consistent with literature for large nozzle orifices and is maintained even when decreasing O_2 concentration up to 15%.

From these conclusions, L10D3G4.28 can be identified as an

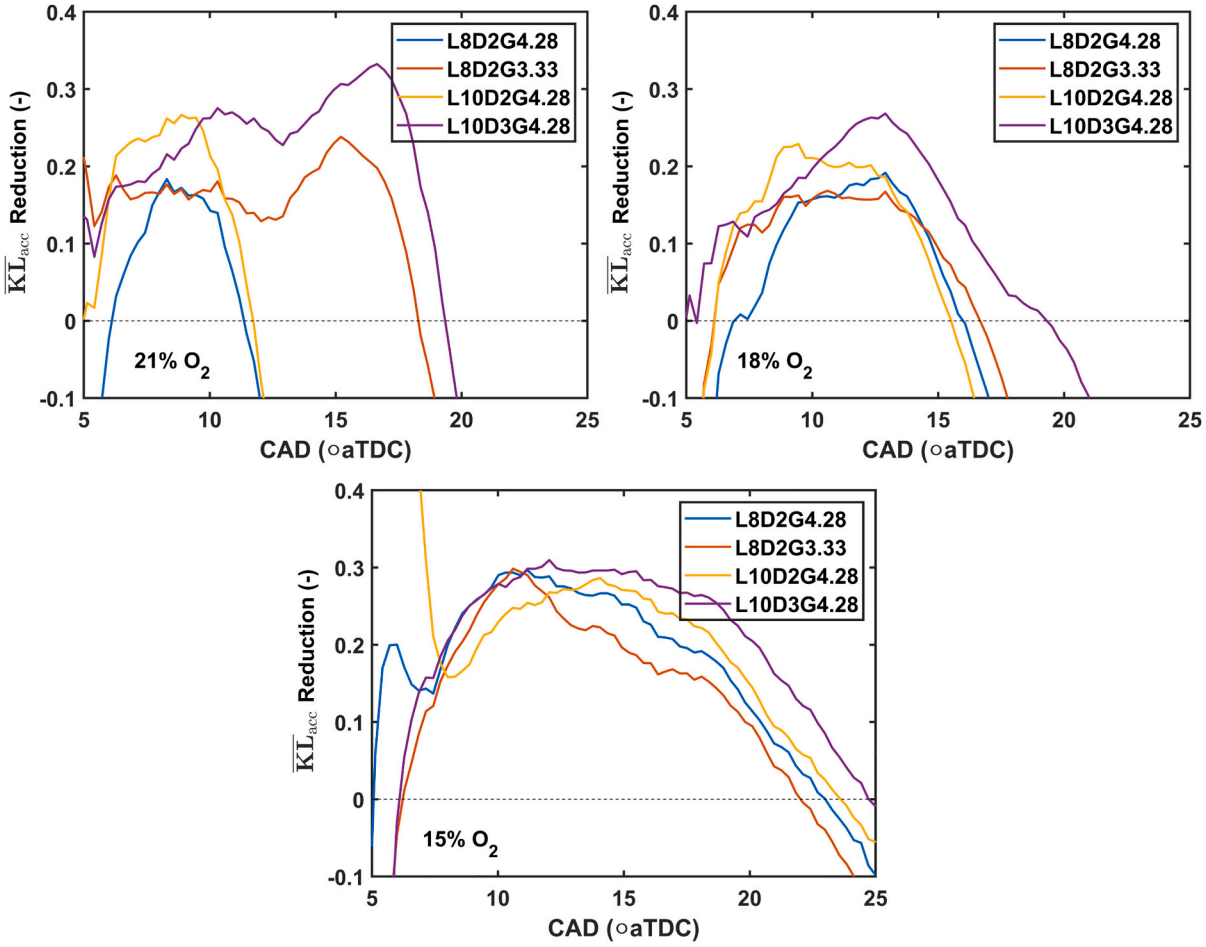

Fig. 13. Mean Accumulated KL ($\overline{KL}_{acc}$) reduction obtained for each duct with respect to Free Spray case at all three oxygen concentrations (21, 18 and 15%).

optimum duct geometry as it provides lowest soot formation and faster oxidation than the other designs. L10D3G4.28 duct effectively reduced around 30–35% of soot (based on KL) with respect to Free spray. However, a further combination of the designs proposed here could perform better. A lower G (3.33 mm) combined with a shorter duct length (8 mm) and larger diameter (3 mm) seems to be the way to find the optimum design for this application. Further exploration in this regard would be required to improve this definition.

Based on the results reported, it can be stated that DFI does reduce net soot formation. However, reduction levels achieved (based on KL) are not as high as those reported in literature. The use of a relatively small-bore size compared to other applications could be a critical aspect as well as the amount of nozzle orifices. Further, the late oxidation problems reported in this work were not observed previously in other scenarios. Therefore, this stage of the combustion process would require a deeper investigation in future works to better understand the reasons after these observations.

CRediT authorship contribution statement

José V. Pastor: Supervision, Resources, Project administration, Funding acquisition, Conceptualization. **Carlos Micó:** Writing – review & editing, Validation, Supervision, Methodology, Formal analysis, Conceptualization. **Felipe Lewiski:** Writing – review & editing, Validation, Software, Formal analysis. **Usama Bin-Khalid:** Writing – review & editing, Writing – original draft, Visualization, Validation, Software, Methodology, Investigation, Formal analysis.

Declaration of competing interest

The authors declare that they have no known competing financial interests or personal relationships that could have appeared to influence the work reported in this paper.

Data availability

No data was used for the research described in the article.

Acknowledgement

This work has been partially funded by Universitat Politècnica de València through grant agreement UPV Subprograma 2 (PAID-01-22).

References

[1] Mueller CJ, Nilsen CW, Ruth DJ, Gehmlich RK, Pickett LM, Skeen SA. Ducted fuel injection: a new approach for lowering soot emissions from direct-injection engines. Appl Energy Oct. 2017;204:206–20. https://doi.org/10.1016/j.apenergy.2017.07.001.

[2] Gehmlich RK, Mueller CJ, Ruth DJ, Nilsen CW, Skeen SA, Manin J. Using ducted fuel injection to attenuate or prevent soot formation in mixing-controlled combustion strategies for engine applications. Appl Energy Sep. 2018;226:1169–86. https://doi.org/10.1016/j.apenergy.2018.05.078.

[3] Fitzgerald RP, Svensson K, Martin G, Qi Y, Koci C. Early Investigation of Ducted Fuel Injection for Reducing Soot in Mixing-Controlled Diesel Flames. SAE Int J Engines Apr. 2018;11(6). https://doi.org/10.4271/2018-01-0238. 2018–01–0238.

[4] Li F, Lee C, Wu H, Wang Z, Liu F. An optical investigation on spray macroscopic characteristics of ducted fuel injection. Exp Therm Fluid Sci Dec. 2019;109:109918. https://doi.org/10.1016/j.expthermflusci.2019.109918.

[5] Fitzgerald R, Svensson K, Martin G. Mixture Fraction Measurements of Diesel Sprays with Ducted Fuel Injection. Int Conf Liquid Atomization Spray Systems (ICLASS) Aug. 2021;1(1). https://doi.org/10.2218/iclass.2021.5939.
[6] Millo F, et al. Ducted fuel injection: experimental and numerical investigation on fuel spray characteristics, air/fuel mixing and soot mitigation potential. Fuel Apr. 2021;289:119835. https://doi.org/10.1016/j.fuel.2020.119835.
[7] Segatori C, Piano A, Peiretti Paradisi B, Bianco A, Millo F. Exploiting the potential of large eddy simulations (LES) for ducted fuel injection investigation in non-reacting conditions. Int J Multiphase Flow Jan. 2024;171:104686. https://doi.org/10.1016/j.ijmultiphaseflow.2023.104686.
[8] Svensson KI, Martin GC. Ducted Fuel Injection: Effects of Stand-Off Distance and Duct Length on Soot Reduction. SAE Int J Adv Curr Pract Mobil Apr. 2019;1(3). https://doi.org/10.4271/2019-01-0545. 2019–01–0545.
[9] Li F, Lee C, Wang Z, Pei Y, Lu G. Impacts of duct inner diameter and standoff distance on macroscopic spray characteristics of ducted fuel injection under non-vaporizing conditions. Int J Engine Res May 2021;22(5):1702–13. https://doi.org/10.1177/1468087420914714.
[10] Nilsen CW, Biles DE, Mueller CJ. Using ducted fuel injection to attenuate soot formation in a mixing-controlled compression ignition engine. SAE Int J Engines May 2019;12(3). https://doi.org/10.4271/03-12-03-0021. 03-12-03–0021.
[11] Li F, Lee C, Wang Z, Liu F, Lu G. Optical investigation on impacts of ambient pressure on macroscopic spray characteristics of ducted fuel injection under non-vaporizing conditions. Fuel May 2020;268:117192. https://doi.org/10.1016/j.fuel.2020.117192.
[12] Svensson K, Fitzgerald R, Martin G. Ducted fuel injection: An experimental study on optimal duct size. Mar. 2022. https://doi.org/10.4271/2022-01-0450.
[13] Nilsen CW, Biles DE, Yraguen BF, Mueller CJ. Ducted fuel injection versus conventional diesel combustion: an operating-parameter sensitivity study conducted in an optical engine with a four-orifice fuel injector. SAE Int J Engines Apr. 2020;13(3). https://doi.org/10.4271/03-13-03-0023. 03-13-03–0023.
[14] Wilmer BM, Nilsen CW, Biles DE, Mueller CJ, Northrop WF. Solid particulate mass and number from ducted fuel injection in an optically accessible diesel engine in skip-fired operation. Int J Engine Res Jul. 2022;23(7):1226–36. https://doi.org/10.1177/14680874211010560.
[15] Svensson K, Kim C, Seiler P, Martin G, Koci C. Performance and emission results from a heavy-duty diesel engine with ducted fuel injection. Apr. 2021. https://doi.org/10.4271/2021-01-0503.
[16] Mueller CJ, Nilsen CW, Biles DE, Yraguen BF. Effects of fuel oxygenation and ducted fuel injection on the performance of a mixing-controlled compression-ignition optical engine with a two-orifice fuel injector. Appl Energy Combust Sci Jun. 2021;6:100024. https://doi.org/10.1016/j.jaecs.2021.100024.
[17] Nyrenstedt G, Nilsen CW, Biles DE, Mueller CJ. Ducted fuel injection with low-net-carbon fuels as a solution for meeting future emissions regulations. Fuel Apr. 2023;338:127167. https://doi.org/10.1016/j.fuel.2022.127167.
[18] Liu X, Mohan B, Im HG. Numerical investigation of the free and ducted fuel injections under compression ignition conditions. Energy Fuel Nov. 2020;34(11):14832–42. https://doi.org/10.1021/acs.energyfuels.0c02757.
[19] Piano A, Segatori C, Millo F, Pesce FC, Vassallo AL. Investigation of ducted fuel injection implementation in a retrofitted light-duty diesel engine through numerical simulation. SAE Int J Engines Nov. 2022;16(5). https://doi.org/10.4271/03-16-05-0038. 03-16-05–0038.
[20] Şener R. Ducted fuel injection: numerical study of soot formation and oxidation using detailed soot modeling approach in a compression ignition engine at different loads. J Brazilian Soc Mech Sci Eng Jan. 2022;44(1):45. https://doi.org/10.1007/s40430-021-03356-z.
[21] Numerical investigation of ducted fuel injection strategy for soot reduction in compression ignition engine. J Appl Fluid Mech Mar. 2022;15(2). https://doi.org/10.47176/jafm.15.02.33088.
[22] Pastor JV, et al. Influence of the radial-lip concept design to achieve ultra-low soot emission reductions: an optical analysis. Fuel Aug. 2023;345:128161. https://doi.org/10.1016/j.fuel.2023.128161.
[23] García-Oliver JM, Novella R, Micó C, Bin-Khalid U. A numerical investigation of the performance of oxymethylene ethers blended with fossil diesel to reduce soot emissions in compression ignition engines. Fuel Sep. 2022;324:124768. https://doi.org/10.1016/j.fuel.2022.124768.
[24] Garcia-Oliver JM, Novella R, Lopez Pintor D, Micó C, Bin-Khalid U. A numerical approach for the analysis of Hydrotreated vegetable oil and dimethoxy methane blends as low-carbon alternative fuel in compression ignition engines. Apr. 2023. https://doi.org/10.4271/2023-01-0338.
[25] García-Oliver JM, Novella R, Micó C, Bin-Khalid U, Lopez-Pintor D. A numerical analysis of hydrotreated vegetable oil and dimethoxymethane (OME_1) blends combustion and pollutant formation through the development of a reduced reaction mechanism. Int J Engine Res Feb. 2024. https://doi.org/10.1177/14680874231226321.
[26] Internal combustion engine fundamentals. 26; 1988. https://doi.org/10.5860/CHOICE.26-0943.
[27] Higgins B, Siebers DL. Measurement of the flame lift-off location on DI diesel sprays using OH Chemiluminescence. Mar. 2001. https://doi.org/10.4271/2001-01-0918.
[28] Riedl MJ. Optical design fundamentals for infrared systems. Second Edition SPIE 2001. https://doi.org/10.1117/3.412729.
[29] Piano A, et al. Numerical and optical soot characterization through 2-color pyrometry technique for an innovative diesel piston bowl design. Fuel Feb. 2023;333:126347. https://doi.org/10.1016/j.fuel.2022.126347.
[30] Pastor JV, Garcia A, Micó C, Lewiski F. An optical investigation of Fischer-Tropsch diesel and Oxymethylene dimethyl ether impact on combustion process for CI engines. Appl Energy 2020;260:114238. https://doi.org/10.1016/j.apenergy.2019.114238.
[31] Pastor JV, García A, Micó C, Lewiski F. Soot reduction for cleaner compression ignition engines through innovative bowl templates. Int J Engine Res Aug. 2021;22(8):2477–91. https://doi.org/10.1177/1468087420951324.
[32] Pastor JV, García-Oliver JM, García A, Micó C, Möller S. Application of optical diagnostics to the quantification of soot in n-alkane flames under diesel conditions. Combust Flame Feb. 2016;164:212–23. https://doi.org/10.1016/j.combustflame.2015.11.018.
[33] Nilsen CW, Biles DE, Wilmer BM, Mueller CJ. Investigating the effects of duct length and diameter and fuel-injector orifice diameter in a compression-ignition engine equipped with ducted fuel injection. Appl Energy Combust Sci Sep. 2021;7:100030. https://doi.org/10.1016/j.jaecs.2021.100030.